Enhanced Fluorescence Detection on Homogeneous Gold Colloid Self-Assembled Monolayer Substrates

Fang Xie,[†] Mark S. Baker,[‡] and Ewa M. Goldys*,[†]

Division of Information and Communication Sciences, Macquarie University, Sydney NSW 2109, Australia, Australian Proteome Analysis Facility Ltd & Department of Chemistry and Biomolecular Science, Macquarie University, Sydney NSW 2109, Australia

Received November 1, 2007. Revised Manuscript Received January 2, 2008

We report the observation of appreciable enhancement of fluorescence induced by large Au colloids on a solid support. Au colloids 40, 59, and 81 nm in radius were homogeneously deposited on glass substrates with varying average particle distances and interparticle coupling. The fluorescence enhancement was examined by using self-assembled monolayers of two different fluorophore−protein conjugates: fluorescein isothiocyanate−human serum albumin (FITC-HSA) and epicocconone (Deep Purple)−bovine serum albumin (DP-BSA). We demonstrated strong variations of fluorescence enhancement with both interparticle distance and particle size. The highest observed fluorescence enhancement for DP-BSA was 15 times with the 162 nm Au colloid and an average interparticle distance of 67 nm, estimated from the particle density in the SEM images. We analyzed the origin of such large enhancement observed for optimized nanoparticle size and distance. To this aim, we separated the effect of the increased excitation rate from the electromagnetic field locally enhanced by the interaction of incident light with the nanoparticles from the effect of higher quantum yield due to an increase of the intrinsic decay rate of the fluorophore. We also demonstrated that the Au colloid monolayers on glass surfaces have outstanding macroscopic homogeneity. This important feature will pave the way for the application of our substrates for ultrasensitive bioassays and similar applications in biotechnology and life sciences.

Introduction

Fluorescence is rapidly becoming a leading methodology in life sciences[1] because of its versatility, potential for multiplexing, ease of use, and remarkable sensitivity. Apart from fluorophore stability, the detection limit of a fluorophore is determined by the ratio of its signal to the background emission due to unavoidable sample autofluorescence. Therefore high fluorophore brightness is a critical requirement for fluorescence detection of trace analytes, especially in the presence of any interfering background fluorescence, and a range of methods have been developed to increase the sensitivity of fluorescence detection.[2–8] Fluorescence amplification by metal nanostructures is a relatively new methodology that has been explored extensively over only the last 5 years. The studies of the effects of metallic surfaces on fluorescence date back to the seventies,[9,10] and the most recent advances in this area and applications in biotechnology were reviewed by Lakowicz et al.[11–14] The phenomenon of metal induced fluorescence enhancement (MIFE) is attributed to interaction of the excited fluorophores with surface plasmon resonances in metals, which is particularly prominent in metal nanostructures. Such structures are able to produce desirable effects such as increased fluorescence quantum yield, decreased lifetime, increased fluorophore photostability, and improved energy transfer.[14] However, when fluorophores are very close to the metal surface, the fluorescence quenching effect competes with these favorable effects[15] and it dominates within 5 nm from the surface of metallic particles. At larger distances the enhancement starts to override the quenching and reaches its maximum at about 10 nm from the metal surface.[16,17] At larger metal−fluorophore separation, the enhancement effect progressively decreases.

* Corresponding author. E-mail: goldys@ics.mq.edu.au.
[†] Division of Information and Communication Sciences, Macquarie University.
[‡] Proteome Analysis Facility Ltd & Department of Chemistry and Biomolecular Science, Macquarie University.

(1) Lakowicz, J. R. *Probe Design and Chemical Sensing*; Lakowicz, J. R., Ed.; Plenum Press: New York, 1994; Vol. 4.
(2) Kronick, M. N. *J. Immunol. Methods* **1986**, *92*, 1.
(3) Gosling, J. P. A. *Cell* **1990**, *36*, 1408.
(4) Lövgen, T.; Pettersson K. *Fluorescence Immunoassay and Molecular Applications*; Van Dyke, K., Van Dyke, R., Eds.; CRC Press: Boca Raton, FL, 1990; pp 234–250.
(5) Casay, G. A.; Shealy, D. B.; Patonay, G. *Probe Design and Chemical Sensing*; Lakowicz, J. R., Ed.; Plenum Press: New York, 1994; Vol. 4.
(6) He, L.; Musick, M. D.; Nicewarner, S. R.; Salinas, F. G.; Benkovic, S. J.; Natan, M. J.; Keating, C. D. *J. Am. Chem. Soc.* **2000**, *122*, 9071.
(7) *Near-Infrared Dyes for High Technology Applications*; Daehne, S.; Resch-Genger, U.; Wolfbeis, O. S., Eds.; Kluwer Academic Publishers: Dordrecht, The Netherlands, 1998.
(8) Walker, N. J. *Science* **2002**, *296*, 557.
(9) Drexhage, K. H. *J. Luminesc.* **1970**, *12*, 693.
(10) Ford, G. W.; Weber, W. H. *Surf. Sci.* **1981**, *109*, 451.
(11) Lakowicz, J. R.; Geddes, C. D.; Gryczynski, I.; Malicka, J.; Gryczynski, Z.; Aslan, K.; Lukomska, J.; Matveeva, E.; Zhang, J.; Badugu, R.; Huang, J. *J. Fluoresc.* **2004**, *14*, 425.
(12) Aslan, K.; Lakowicz, J. R.; Geddes, C. D. *Anal. Bioanal. Chem.* **2005**, *382*, 926.
(13) Alsan, K.; Gryczynski, I.; Malicka, J.; Matveeva, E.; Lakowicz, J. R.; Geddes, C. D. *Curr. Opin. Biotechnol.* **2005**, *16*, 55.
(14) Lakowicz, J. R. *Anal. Biochem.* **2005**, *337*, 171.
(15) Kerker, M.; Blatchford, C. G. *Phys. Rev. B* **1982**, *26*, 4082.
(16) Gersten, J. I.; Nitzan, A. *Surf. Sci* **1985**, *158*, 165.
(17) Lakowicz, J. R. *Anal. Biochem.* **2001**, *298*, 1.

10.1021/cm703121m CCC: $40.75
Published on Web 02/06/2008

Various MIFE substrates have been reported in the literature, mostly based on inhomogeneous silver nanoscale structures of various shapes, including silver island films (SiFs),[18] silver colloids,[19,20] silver nanorods,[21] silver triangles,[22] and silver fractal-like nanostructures.[23] In addition to varying the particle shape, different techniques for laying down the nanoparticles, such as electroplating[23] and light-assisted deposition,[24] have also been employed. Nearly all of these MIFE substrates are inhomogeneous, with large spatial variations of the fluorescence enhancement factor. Most recently, periodic arrays of metal nanoparticles[25–27] have been produced by electron beam lithography to ensure uniform fluorescent enhancement. However, the difficulties in producing large-scale active areas by e-beam lithography and high cost prevent their wider applications.

Silver is one of the most frequently used metals for fluorescence enhancement.[14] Silvered surfaces perform well in MIFE applications when stored in water and used within few days after preparation.[28] However, such surfaces deteriorate after long storage times and are prone to oxidation, so their shelf life is limited. Their exposure to air at higher temperatures (used, for example to deactivate biological molecules[28]) accelerates the oxidation process. In contrast, gold surfaces resist oxidation much better and remain stable for many months after preparation. Importantly, gold-based substrates such as Au colloids can be produced with well-controlled and homogeneous coverage. However, earlier authors were able to achieve very limited fluorescence enhancement by using gold, on the order of 3 folds only.[29]

We have been able to identify and overcome the difficulties of producing good-quality gold MIFE substrates through our in-depth analysis of fluorophore behavior close to such metal nanostructures. Our success was based on the realization that the emission of fluorophores located in close proximity (<10 nm) to gold colloids up to 30 nm in diameter is quenched, due to nonradiative energy transfer from the excited states of the fluorophore to gold colloids.[30,31] Considerations based on Mie theory suggest that small particles quench fluorescence because the absorption dominates over the scattering,[14] an effect clearly apparent in the optical extinction spectra. Conversely, large particles can enhance fluorescence more effectively because the scattering component dominates.[14] On these grounds, we hypothesized that large gold colloids would enhance fluorescence as the enhancement effect would override the quenching. Additionally, the exciting electromagnetic field can be amplified in confined regions between sufficiently close nanoparticles, and this effect can further enhance fluorescence. Employing these ideas, we have been able to produce a gold colloid self-assembled monolayer-based MIFE substrate with significantly improved enhancement compared with earlier results[29] and excellent uniformity by using a simple approach. This improvement was achieved by a systematic investigation of the effects of size and interparticle distance on fluorescence enhancement.

In our study, in addition to the widely used fluorophore-FITC,[49] a newly developed fluorophore Deep Purple was also used. The active compound of Deep Purple, epicocconone, is a heterocyclic natural product from the fungus *Epicoccum nigrum* that fluoresces weakly in the green (520 nm). Its fluorescence peak intensity shifts to red (610 nm) with a concomitant increase in quantum yield to 0.2 in the presence of a protein.[32] Deep Purple has been widely used in proteomics in applications such as 1D/2D gel electrophoresis and electroblots and in live cell imaging and multiplexing because of its unique properties such as cellular membrane permeability, long Stokes shift, and major increase in brightness upon binding to proteins.

In this study, Au colloids 40, 59, and 81 nm in radius, were homogeneously deposited on the chemically modified glass surfaces. To this aim, we employed the established technique of self-assembly of Au colloids on glass surfaces, investigated earlier for SERS applications.[33]In this method, (3-aminopropyl)trimethoxylsilane (APTMS) is first chemically bonded to hydroxyl groups on the glass substrate surface. The amino-functional groups present in APTMS facilitate the attachment of gold nanoparticles. Two types of samples were prepared, with large interparticle distance and hence little or no interparticle coupling and small interparticle distance producing effective interparticle coupling. The fluorescence enhancement was investigated by forming a monolayer of FITC-conjugated human serum albumin (FITC-HSA) and Deep Purple-conjugated bovine serum albumin (DP-BSA) both on gold nanoparticle covered glass surface as well as on bare glass surface as a control, respectively. The enhancement factor (E_t) was determined as the ratio of fluorescence intensity on metallic surface to fluorescence intensity on glass. The fluorescence lifetime measurements were also carried out on the self-assembled monolayer of DP-BSA both on a metallic surface and a glass surface as a control. These data reveal high and varying values of fluorescence enhancement factor and strong variations of fluorophore lifetime that depend on interparticle

(18) Lakowicz, J. R.; Shen, Y.; D'Auria, S.; Malicka, J.; Fang, J.; Gryczynski, Z.; Gryczynski, I. *Anal. Biochem.* **2002**, *301*, 261.
(19) Sokolov, K.; Chumanov, G.; Cotton, T. M. *Anal. Chem.* **1998**, *70*, 3898.
(20) Geddes, C. D.; Cao, H.; Gryczynski, I.; Gryczynski, Z.; Fang, J.; Lakowicz, J. R. *J. Phys. Chem. A* **2003**, *107*, 3443.
(21) Aslan, K.; Leonenko, Z.; Lakowicz, J. R.; Geddes, C. D. *J. Phys. Chem. B* **2005**, *109*, 3157.
(22) Aslan, K.; Lakowicz, J. R.; Geddes, C. D. *J. Phys. Chem. B* **2005**, *109*, 6247.
(23) Geddes, C. D.; Parfenov, A.; Roll, D.; Fang, J.; Lalowicz, J. R. *Langmuir* **2003**, *19*, 6236.
(24) Geddes, C. D.; Parfenov, A.; Lakowicz, J. R. *Appl. Spectrosc.* **2003**, *57*, 526.
(25) Corrigan, T. D.; Guo, S.; Phaneuf, R. J.; Szmacinski, H. *J. Fluoresc.* **2005**, *15*, 777.
(26) Chen, Y.; Munechika, K.; Ginger, D. S. *Nano Lett.* **2007**, *7*, 690.
(27) Pompa, P. P.; Martiradonna, L.; Torre, A. D.; Sala, D.; Manna, L.; Vittorio, M. D.; Calabi, F.; Cingolani, R.; Rinaldi, R. *Nat. Nanotechnol.* **2006**, *1*, 126.
(28) Aslan, K.; Leonenko, Z.; Lakowicz, J. R.; Geddes, C. D. *J. Fluoresc.* **2005**, *15*, 643.
(29) Aslan, K.; Malyn, S. N.; Geddes, C. D. *J. Fluoresc.* **2007**, *17*, 7.
(30) Dulkeith, E.; Morteani, A. C.; Niewdereichholz, T.; Klar, T. A.; Feldmann, J.; Levi, S. A.; van Veggel, F.C.J.M.; Reihoudt, D. N.; Moller, M.; Gittins, D. I. *Phys. Rev. Lett.* **2002**, *89*, 203002.
(31) Dulkeith, E.; Ringler, M.; Klar, T. A.; Feldmann, J.; Javier, A. M.; Parak, W. J. *Nano Lett.* **2005**, *5*, 585.
(32) Coghlan, D. R.; Mackintosh, J. A.; Karuso, P. *Org. Lett.* **2005**, *7*, 2401.
(33) Grabar, K. C.; Freeman, R. G.; Hommer, M. B.; Natan, M. J. *Anal. Chem.* **1995**, *67*, 735–743.
(34) Frens, G. *Nat. Phys. Sci.* **1973**, *241*, 20–22.

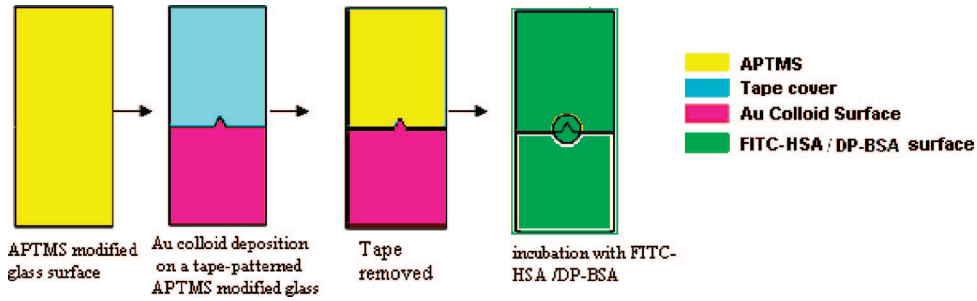

Figure 1. Schematic illustration of the deposition procedure for Au colloid self-assembled monolayer and the formation of fluorophore−protein monolayer. The lifetime images for DP-BSA were collected close to the interface of metal and glass surface (inside the circle).

distance and particle size. As discussed further in this paper, the origin of large enhancement observed for appropriate size nanoparticles with optimized interparticle distance is attributed to the effect of an increased excitation rate from the local field enhanced by the interaction of incident light with the nanoparticles and higher quantum yield from an increase in the intrinsic decay rate of the fluorophore.[14]

Experimental Section

Materials. The following materials were purchased from Sigma-Aldrich and used as received: $HAuCl_4 \cdot 3H_2O$, trisodium citrate dehydrate, (3-aminopropyl)trimethoxylsilane (APTMS), acetic acid, sodium bicarbonate (Na_2CO_3), bovine serum albumin (BSA), and FITC-conjugated human serum albumin (FITC-HSA). Deep Purple total protein stain (Deep Purple) was purchased from GE Healthcare. Concentrated HCl, HNO_3, H_2SO_4, and methanol were obtained from J. T. Baker Inc., and 30% H_2O_2 from VWR. Glass microscope slides were obtained from Fisher Scientific. Nanopure water (>18.0 MΩ), purified using the Millipore Milli-Q gradient system, was used in all experiments.

Au Colloid Synthesis in Aqueous Solution. The Au colloid was synthesized according to the Frens' method with slight modifications.[33] All glassware used in synthesis was thoroughly cleaned in aqua regia (HCl: HNO_3 = 3:1), rinsed with Milli-Q water and oven-dried prior to use. The stock solutions of 1% $HAuCl_4$ and 38.8 mM sodium citrate were prepared in advance. Other solutions were made freshly as needed. During preparation of various sizes Au colloids, 100 mL of 0.01% $HAuCl_4$ was brought to a rolling boil with vigorous stirring in a 500 mL three-neck round-bottom flask with a condenser. One, 0.75, and 0.5 mL of 38.8 mM sodium citrate was rapidly added to the vortex of the solution, respectively, to produce different sizes of Au colloid. Boiling was continued for about 10 min before the heating mantle was removed with vigorous stirring until the solution reached room temperature. The resulting colloidal solution was characterized by UV–visible spectroscopy. Scanning electron microscopy (SEM) showed the particles have an average size of 80 ± 7, 118 ± 11, and 162 ± 17 nm, respectively.

Formation of Au Colloid Monolayer on Glass. The microscope glass slide was first cleaned by a piranha solution consisting of 4 parts H_2SO_4 and 1 part 30% H_2O_2 at 60 °C (**Caution***: Piranha solution is extremely caustic. Use only with extreme care.*). The glass surface was then derivatized with organosilane APTMS by immersing it into 10 mM methanolic solution.[33] After 2 h, the substrate was removed and rinsed with CH_3OH to remove unbound monomers from the surface. Prior to derivatization with Au colloid, the glass substrate was rinsed thoroughly with water and then immersed in the Au colloid solution to form a monolayer of Au nanoparticles on the glass surface. Depending on time and concentration of the Au colloid solution used, Au nanoparticle layers with various interparticle distances were formed on glass. In our experiments, two types of samples were prepared. Two hours incubation of the APTMS-modified glass surface in the colloidal solution produced Au colloid monolayers with large interparticle distance and hence little or no interparticle coupling. After 24 h incubation Au monolayers with small interparticle distance were formed with effective interparticle coupling. Finally the samples were rinsed with water and dried in N_2.

Fluorophore−Protein Conjugation Monolayer Formation. We selected the fluorophore−protein conjugates (FITC-HSA and DP-BSA) for this study, based on earlier reports that albumin proteins spontaneously bind to glass and silver/gold surfaces to form a complete monolayer.[35] Binding of FITC-HSA to the gold colloidal surface or, in control experiments to the glass surface, was carried out by incubating the surfaces in a 10 μM FITC-HSA solution overnight at 4 °C, followed by rinsing with buffer to remove the unbound materials. In order to deposit a DP-BSA monolayer, a BSA monolayer was first formed on the gold colloid/glass surface by incubating the surfaces in a 10 μg/mL BSA solution overnight at 4 °C, followed by rinsing with buffer to remove the unbound BSA molecules. Deep Purple fluorophore was then conjugated to BSA monolayers by incubation of the modified substrate in 1:200 Deep Purple buffered solution at pH 7 for 1 h at room temperature. Unconjugated Deep Purple was removed by rinsing the substrate with the solution of 15% methanol and 7.5% acetic acid.[32]

Methods. As illustrated in Figure 1, the glass slide was cut to approximately 20 mm × 7 mm in size to fit into 2 mL Eppendorf tube for derivatization. After derivatization with APTMS, the glass surface was patterned by an adhesive tape cut into a V shape as shown in Figure 1. Following the Au colloid self-assembly step, both the glass and Au colloid deposited surfaces were exposed to FITC-HSA and DP-BSA by incubation in the respective solutions, where a 4 nm thick protein monolayer was formed.[36] This fluorescent monolayer makes it possible to quantitatively compare the fluorescence intensity of fluorophore−protein conjugates with and without gold nanostructures. The fluorescence enhancement factor (E_t) was determined as the ratio of fluorescence peak intensity on gold surface to fluorescence intensity on glass based on the fluorescence spectra, given that both surfaces are known to have almost equal monolayer coverage.[37] The fluorescence lifetime images for DP-BSA were collected at the interface of metal and glass surface, in the vicinity of the triangular cutout (Figure 1).

Characterization. UV–visible extinction spectra were obtained using a Cary 5000 UV–vis-NIR Spectrophotometer. During measurements, the glass substrates were maintained in an upright position in the thin film sample holder. Unpolarized white light

(35) Doron, A.; Katz, E.; Willner, I. *Langmuir* **1995**, *11*, 1313.
(36) Lakowicz, J. R.; Malicka, J.; D'Auria, S.; Gryczynski, I. *Anal. Biochem.* **2003**, *320*, 13.
(37) Malicka, J.; Gryczynski, I.; Geddes, C. D.; Lakowicz, J. R. *J. Biomed. Opt.* **2003**, *8* (3), 472.

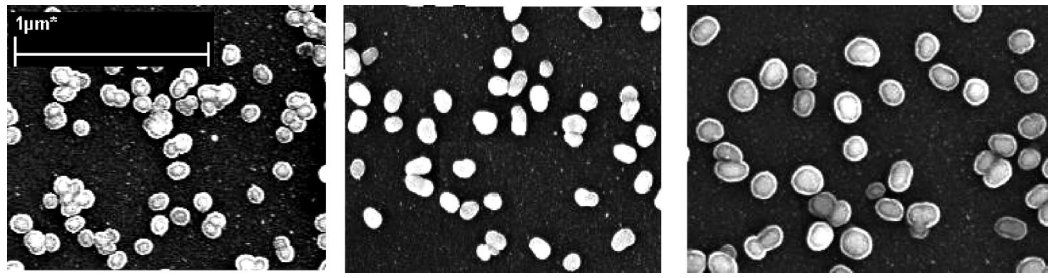

Figure 2. SEM images of (A) 80 nm Au colloid; (B) 118 nm Au colloid; (C) 162 nm Au colloid after 24 h deposition onto the APTMS modified glass substrates. All images were taken at the same magnification (50 K).

from a tungsten halogen lamp was focused on the sample to a spot size of ~1 mm. Scanning electronic microscopy images were collected using a scanning electronic microscope (Joel-JEM-1200 EX II electron microscope). All the samples examined by SEM were coated with 10 nm amorphous carbon, which contributed to the apparent nanoparticle size. Fluorescence emission spectra were taken by a Fluorolog Tau 3 system from Jobin-Yvon-Horiba with 450W Xe lamp excitation. The spectral width was set to 8 nm. All spectra were corrected for system response. To minimize the contribution of scattering of excitation light from the Au nanoparticle surface, we fixed the sample in a sample holder at a 60° angle of incidence. For the samples with FITC-HSA monolayers, the emission spectra were excited at 470 nm and recorded over a range of 490−600 nm. For the samples with DP-BSA monolayers, the fluorescence emission spectra were excited at 514 nm and collected over a range of 540−650 nm. The lifetime measurements were taken by using a laser scanning microscopy SPM2 system (Leica Microsystems) equipped with fluorescence lifetime imaging (FLIM) based on a time-correlated single photon counting (TCSPC) module from Becker & Hickl (SPC-830). The system time resolution is 25 ps and the measurable lifetime range is from 50 ps to 30 ns. In FLIM measurements, a representative sample area of about 55 μm × 55 μm was excited using a 405 nm pulsed laser diode modulated at the frequency of 40 MHz. The fluorescence signal passing through the Airy pinhole was detected by using the SPC-830 module with 256 × 256 channels at 256 ADC resolution, forming a FLIM image with spatial resolution corresponding to number of channels, that is 256 × 256 pixels.

Results and Discussion

Characterization of the MIFE substrates. The SEM images (Figure 2) of gold nanoparticles on the slides were recorded and their size distributions were obtained from at least 200 individual particles using the Scion Image beta software release 2 (available at www.scioncorp.com). The Au colloid had average diameters of 80 ± 7, 118 ± 11, and 162 ± 17 nm, respectively, implying that Au colloid solutions were practically monodisperse. The scanning electron micrographs also show that the nanoparticles are approximately spherical and uniformly dispersed in a single layer on the glass surface. After 2 h incubation time, the interparticle distances in the layers are about 310, 480, and 550 nm for the respective Au colloid sizes. These were obtained from the nanoparticle densities observed on the SEM images. As the center-to-center spacings are more than 2–3 times the particle size, in this group of slides, the interparticle coupling is practically absent.[38] In contrast, for the samples with 24 h incubation time, individual particles in the self-assembled layer have small interparticle distances (55, 96, and 67 nm), which lead to effective coupling as the electromagnetic interaction is stronger. However, the main contribution to the effective electromagnetic coupling is due to the lower end of the interparticle distance distribution as the coupling is strongly increased at small interparticle distances. The self-assembled Au monolayers thus prepared are stable because of several factors. First, the Au colloid tends to tightly bind to the glass surface as numerous bonds are formed between Au colloid and substrate surface. The density of these bonds is reported to be high, approximately 4.5 hydroxyl groups per one square nanometer of the glass surface.[39] For a 80 nm diameter nanoparticle with an approximately 40 × 40 nm^2 effective contact area, this produces over 7000 linkages leading to strong binding of the nanoparticles to glass.[26] Second, the thermodynamic stability of these surfaces is very high, thus the exchange with molecules in solution containing the same functional group practically does not occur.[33] Strong covalent bonds to the glass substrate also reduce the surface mobility of the nanoparticles and thus prevent their spontaneous coalescence. The UV–visible spectroscopy was used to record optical properties of the Au colloids monolayers with various interparticle distances. The immobilized Au nanoparticles on glass surface showed characteristic surface plasmon peaks (Figure 3). [33] With increasing deposition time, the optical density accordingly increased, this effect was observed for each size of Au colloid. As shown in Figure 3, the peak position remains unchanged for different incubation times and there is no apparent change in the fwhm, indicating that, for each size of Au colloid, the monolayers with small and large interparticle distances do not experience large-scale aggregation.

In our method, an adhesive tape was used to pattern the APTMS modified glass surface, hence the need to prove a negligible effect of this process on the amount of FITC-HSA binding. This was verified in the experiment, where half of the APTMS-modified glass slide was covered by tape which was then removed. Afterward, the entire slide was incubated

(38) Corrigan, T. D.; Guo, S. H.; Szmacinski, H.; Phaneuf, R. J. *Appl. Phys. Lett.* **2006**, *88*, 101112.
(39) Kruger, A. A. *Surface and Near-Surface Chemistry of Oxide Materials*; Nowotny, J., Dufour, L. C., Eds., Elsevier Science Publishers: Amsterdam 1988; pp 413–448.
(40) Kreirib, U.; Vollmer, M.; *Optical Properties of Metal Clusters*; Springer: Berlin, 1995, p. 532.
(41) Feldheim, D. L.; Foss, C. A. *Metal Nanoparticles: Synthesis, Characterization and Applications*; Marcel Dekker: New York, 2002, p. 338.
(42) Kerker, M.; Blatchford, C. G. *Phys. Rev. B* **1982**, *26*, 8–4052.

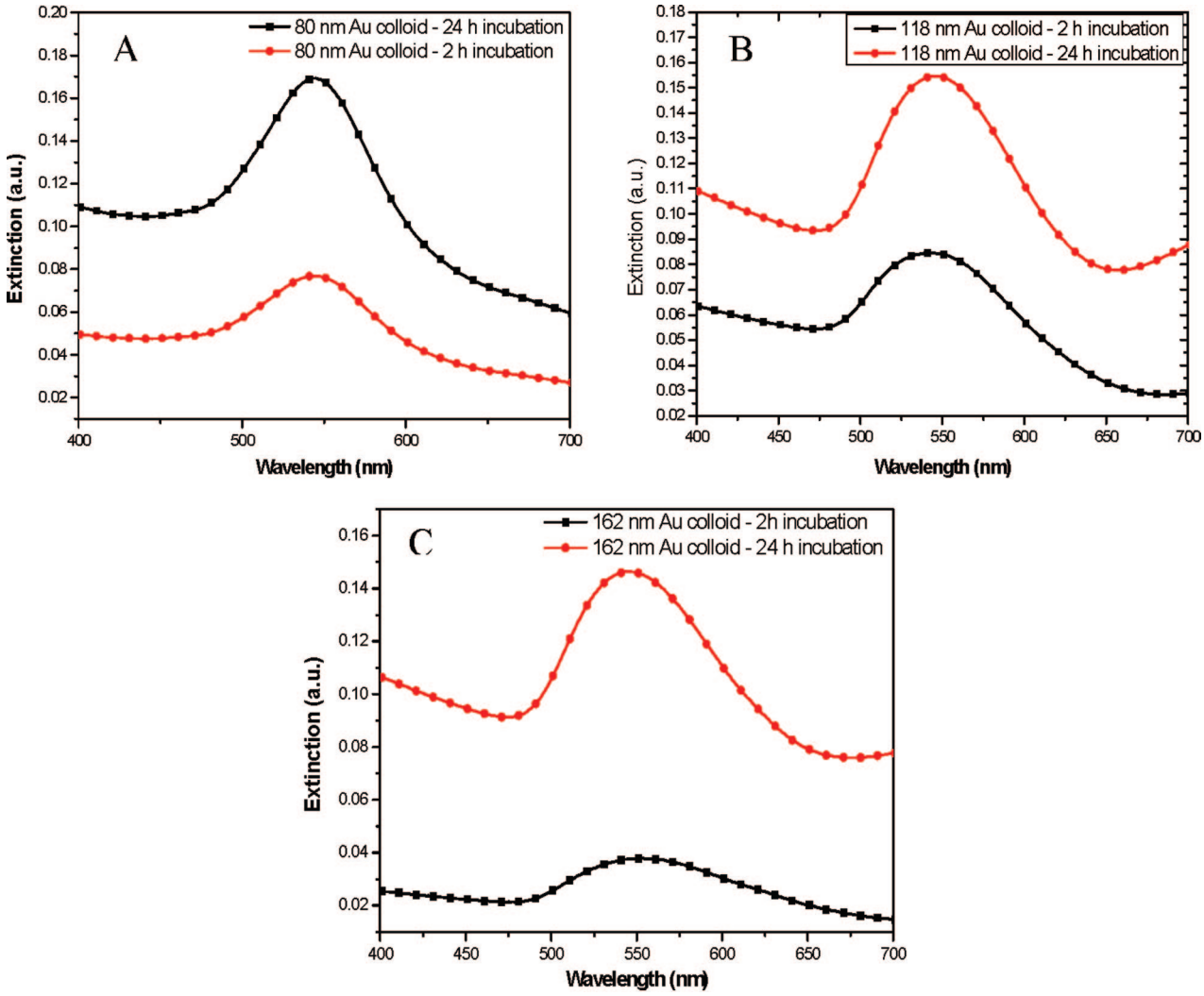

Figure 3. UV–visible spectra for (A) 2 and 24 h incubation of 80 nm Au colloid on glass substrate; (B) 2 and 24 h incubation of 118 nm Au colloid; (C) 2 and 24 h incubation of 162 nm Au colloid.

in the FITC-HSA solution overnight at 4 °C and characterized by laser scanning microscopy with excitation at 488 nm. The image (not shown) revealed identical fluorescence intensity of both untouched and previously covered halves of the slide, suggesting the same amount of protein−dye conjugation and hence the validity of our method.

Fluorescence Enhancement from the FITC-HSA Monolayers. Panels A and B in Figure 4 show the fluorescence spectra from FITC-HSA monolayers on samples with 2 and 24 h incubation. The data were taken for each size Au colloids monolayers, as well as for a control sample with a clean glass surface. The enhancement factors as obtained from these spectra for the samples with 2 h incubation time are 3.8, 5.0, and 5.9 for 80, 118, and 162 nm Au colloid, respectively, and there was little variation between different spots on the surface. After 24 h incubation where interparticle distances are much lower, the fluorescence enhancement factors significantly increase to 5.3, 8.1, and 11.8 for 80, 118, and 162 nm Au colloids, respectively. Figure 4C shows the normalized emission intensities of FITC-HSA on glass and on gold colloid-coated surface, indicating that the spectral characteristics of FITC are unchanged. These results demonstrate that the fluorescence intensities were increased on the colloid-coated surface and the enhancement values were higher in samples with high density of Au colloids, both of which are in good agreement with earlier references.[14,43,45] Such effect of nanoparticles on fluorescence is attributed to the interplay of two principal factors: the change of excitation rate caused by local electromagnetic field enhanced by the interaction of an incident light with the metal nanoparticles and the change of quantum yield due to the effect of metals on the intrinsic decay rate of the fluorophore.[11] This interplay depends strongly on the size and shape of the metal nanoparticles, the interparticle distance, and the spectral relationship between the native fluorescence emission from fluorophore and the extinction spectra of the metal nanoparticles.[46] These are now discussed in more detail.

The effect of Au colloid size on the fluorescence enhancement is attributed to size-dependent extinction properties of metal particles. For a spherical metal particle with size comparable to the incident wavelength, these can be reason-

(43) Ygurabide, J.; Ygurabide, E. *Anal. Biochem.* **1998**, *262*, 137.
(44) Ygurabide, J.; Ygurabide, E. *Anal. Biochem.* **1998**, *262*, 157.
(45) Messinger, B. J.; Raben, U.; Chang, R. K.; Barber, P. W. *Phys. Rev. B,* **1981**, *24*, 2–649.
(46) Song, J.; Atay, T.; Shi, S.; Urabe, H.; Nurmikko, A. V. *Nano Lett.* **2005**, *5*, 1557.

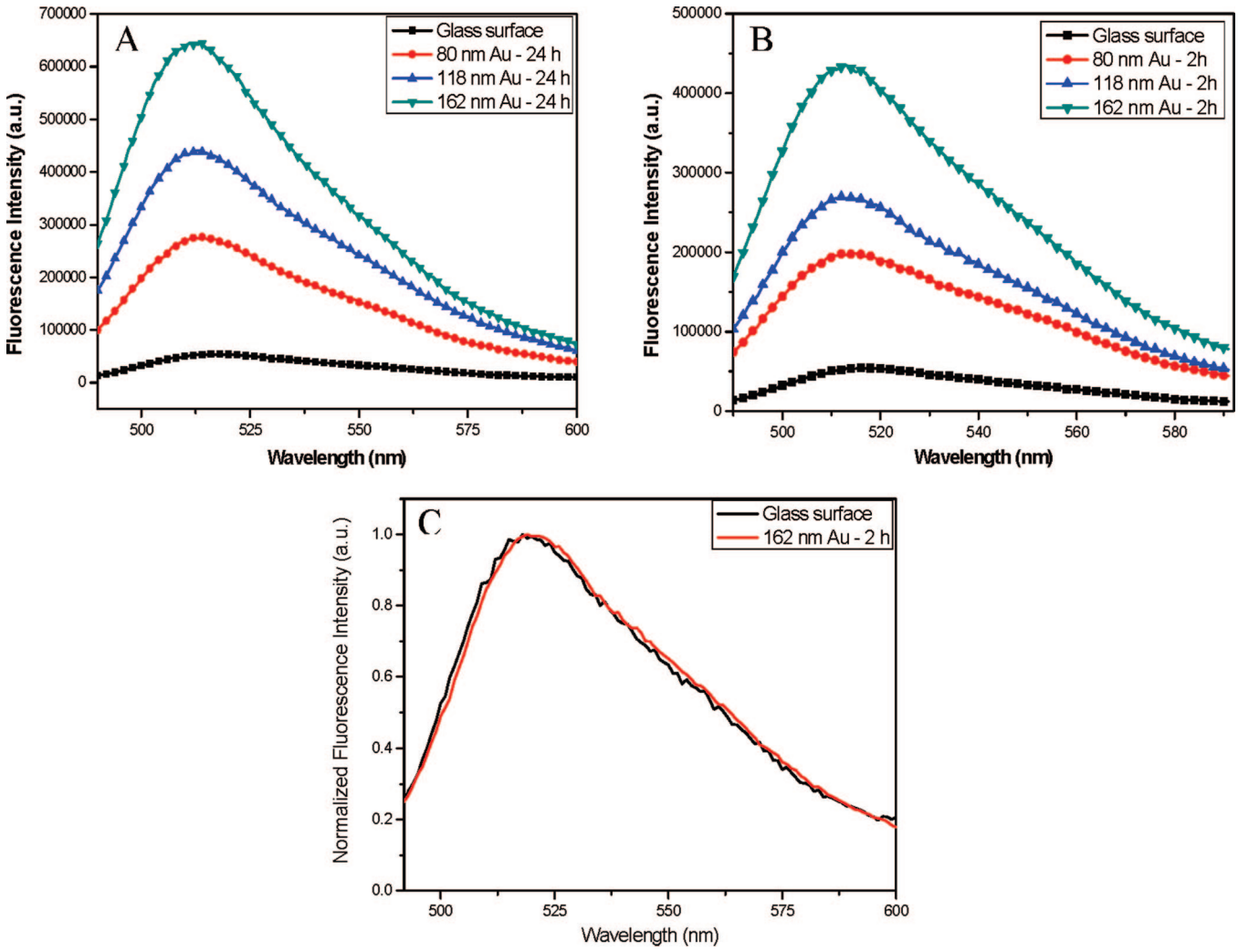

Figure 4. Fluorescence emission intensity of FITC-HSA (A) on substrate with 2 h incubation time (from top to bottom): 162 nm Au colloid; 118 nm Au colloid; and 80 nm Au colloid; (B) on substrate with 24 h incubation time (from top to bottom): 162 nm Au colloid; 118 nm Au colloid; and 80 nm Au colloid. (C) Normalized emission spectra of FITC-HSA on glass and on metallic surface.

ably well described by the Mie theory,[14] which predicts the extinction cross section for a particle with a dielectric constant ϵ_1, to be given by

$$C_E = C_A + C_S \quad (1)$$

where $C_A = k_1 \mathrm{Im}(\alpha)$, $C_S = k_1^4 |\alpha|^2 / 6\pi$, $k_1 = 2\pi n_1/\lambda_0$ is the wavevector of the incident light in the surrounding medium, and α is the polarizability of the sphere of radius r,

$$\alpha = r^3(\epsilon_m - \epsilon_1)/(\epsilon_m + 2\epsilon_1) \quad (2)$$

Here, ϵ_m and ϵ_1 are the complex dielectric constants of the metal and the surrounding medium.

The extinction cross-section comprises two terms C_A and C_S, reflecting absorption and scattering.[40–44] The absorption component of the extinction, C_A, relates to fluorescence quenching.[14] In contrast, the scattering component, C_S, relates to extent by which the plasmons can radiate the energy as a far-field propagating wave and is linked to fluorescence enhancement.[11] Equations 1 and 2 show that C_A increases as r^3, whereas C_S increases as r^6, which implies that small metal particles are expected to quench fluorescence because absorption dominates over the scattering, whereas larger metal particles are expected to enhance fluorescence because the scattering component is more significant than absorption.

On the basis of these considerations, the effect of Au colloid size on fluorescence enhancement can be correlated with the scattering and absorption components of the extinction spectra (Figure 3). A convenient measure is the scattering quantum yield, φ_s, defined as $\varphi_s = C_S/C_E = C_S/(C_A + C_S)$. By using C_S, C_A, and C_E given by eq 1, we calculate the values of φ_s for 80, 118, and 162 nm Au colloids to be 0.53, 0.88, and 0.98, respectively.[35] This increase in the scattering quantum yield is in the agreement with our experimentally observed increases of fluorescence enhancement factors with Au colloid size for both 2 and 24 h incubation time.

We note that the observed increase of fluorescence intensity, in principle, can be due to geometrical effects such as an increased surface area, given the same fluorophore coverage on both colloid-coated and glass surface.[19–22] We have accounted for such geometrical factors by calculating the total radiant flux emitted by the fluorophore layer covering our nanostructures. This is a more exact approach compared with the calculation of the

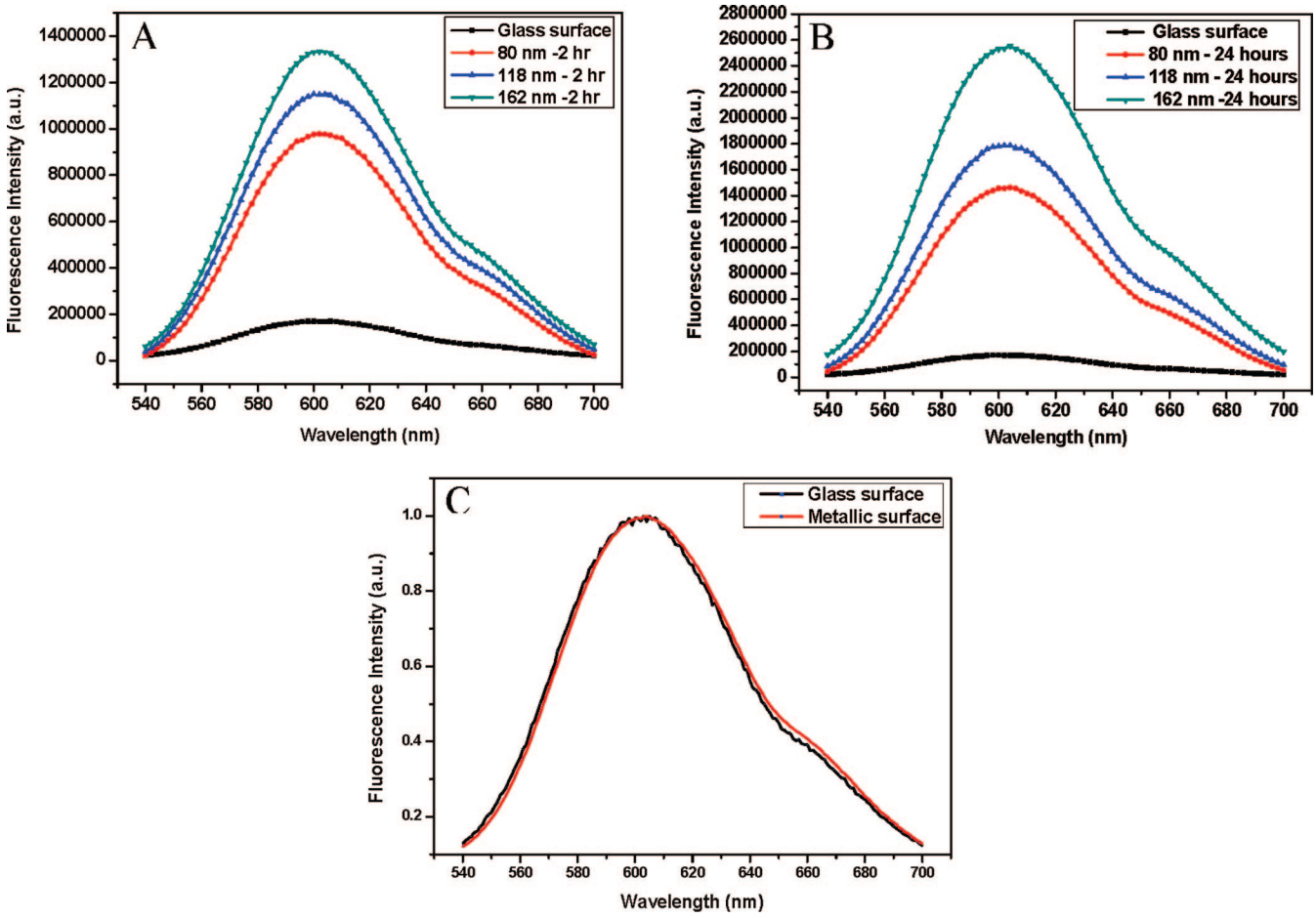

Figure 5. (A) Fluorescence emission intensity of DP-BSA monolayers coating: on 162, 118, and 80 nm Au colloid with 2 h incubation time; (B) fluorescence emission intensity of DP-BSA monolayer coating on 162, 118, and 80 nm Au colloid with 24 h incubation time. (C) Normalized emission spectra of DP-BSA on glass and on 162 nm Au colloid with 24 h incubation time.

surface area. First we calculated the radiant flux emitted by a sphere covered with a uniform fluorescent layer. This layer is illuminated by a parallel exciting light beam, and consequently, the sides of the sphere are not as bright as its top, which has been accounted for appropriate integration. We used a Lambertian source approximation consistent with typical observation conditions. By comparing the radiant flux from such a sphere with the radiant flux emitted by a flat surface in the absence of that sphere, we found that the sphere (despite larger surface area) emits only two-thirds of light that would be emitted by area of the flat surface occupied by that sphere (equal to its cross-section). This means that the presence of spherical nanoparticles deposited on the flat surface does not increase, but slightly decreases the fluorescence intensity, produced by fluorescence monolayer coating.

Fluorescence Enhancement and Lifetime Measurements of the DP-BSA Monolayers. Further we explored fluorescence enhancement of DP-BSA monolayers. Figure 5A and 5B show the fluorescence spectra from DP-BSA monolayers on samples with various sizes of Au colloids and incubation times, and the control sample. The enhancement factors at 24 h incubation time were 15.8, 11.3, and 9.4 for 162, 118, and 80 nm size Au colloids, respectively. The enhancement values decreased in the samples with low densities of Au nanoparticles at 2 h incubation. For such less dense samples with Au colloid sizes of 162, 118, and 80 nm, the enhancement factors were 7.5, 6.7, and 5.7, respectively. The results for DP-BSA are similar to those observed for FITC-HSA monolayers for the same sample preparation conditions.

For the DP-BSA monolayers that can be excited by a pulsed 405 nm laser, we have been able to carry out fluorescence lifetime studies that provide more detailed insights into the fluorescence enhancement process through the fluorescence decay rates. These are important because the enhancement of fluorescence observed on the nanostructured gold surfaces is a result of two effects: an increase of a local electromagnetic field near gold nanoparticles, leading to increased excitation rate of fluorophores and an increase of the radiative decay rate Γ of fluorophores close to metal nanostructures, reflected both in the fluorescence lifetime and quantum yield.[14] The local electromagnetic field enhancement produces a higher excitation rate but it does not change the lifetime of the fluorophore; this effect is referred as excitation enhancement (E_{ex}). The second effect referred as emission enhancement (E_{em}), increases the quantum yield and reduces the lifetime of the fluorophore.[46] Although it is difficult to separate the effects of excitation and emission enhancements, the studies of fluorescence lifetime make it possible to examine these two contributions semiquan-

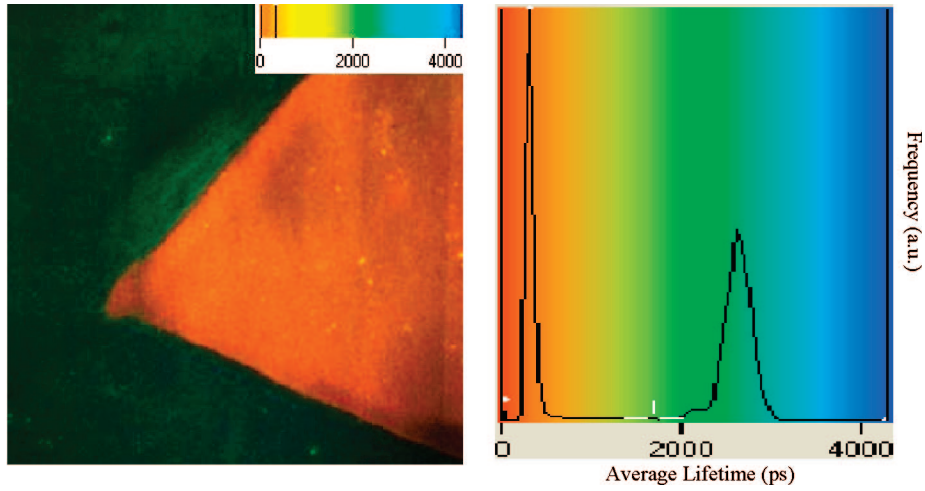

Figure 6. (A) Color-coded lifetime image for the sample with 162 nm Au colloid after 24 h deposition. (The color-coded fluorescence lifetime scale bar is displayed on top-right corner); the triangle is the colloid-coated monolayer, the surrounding area is clean glass surface. The entire sample is covered with a fluorescent DP-BSA monolayer. (B) Distribution of the average lifetime obtained in the FLIM data analysis for metallic and glass area of the same sample. Image area is 2.5 mm × 2.5 mm.

Table 1. Lifetime Measurements for Each Sample and the Calculated Values of Rate, Yield Ratios, and Modified Quantum Yield Q_m; τ is the Average Lifetime Value of the Control Sample (2.6 ns)

sample	τ/τ_m	Γ_m/Γ	$Q_m/Q = E_{em}$	Q_m
162 nm Au − 24 h	8.9	39.5	4.55	0.91
118 nm Au − 24 h	8.6	38.0	4.42	0.90
80 nm Au − 24 h	7.2	31.0	4.40	0.89
162 nm Au − 2 h	4.1	15.5	4.00	0.80
118 nm Au − 2 h	3.2	11.0	3.75	0.75
80 nm Au − 2 h	2.4	7.3	3.35	0.67

Table 2. Values of the Excitation Enhancement and Emission Enhancement for Each Sample

sample	enhancement factor (E_t)	emission enhancement (E_{em})	excitation enhancement (E_{ex})
162 nm Au − 2 h	7.5	4.00	1.88
118 nm Au − 2 h	6.70	3.75	1.78
80 nm Au − 2 h	5.70	3.35	1.70
162 nm Au − 24 h	15.80	4.55	3.47
118 nm Au − 24 h	11.30	4.42	2.56
80 nm Au − 24 h	9.40	4.40	2.14

titatively and separately investigate the effect of both the size and interparticle distance on each.

The fluorescence lifetime images for each sample were collected in the region with an Au colloid-coated triangle area (see Figure 1) and the surrounding glass surface used as a control. The results for the sample with 118 nm Au colloid incubated for 24 h are shown in Figure 6. The fluorescence decay curves collected in each pixel could be satisfactorily fitted using a two component decay model from which an average lifetime value was calculated.[47] The average lifetime for each pixel is displayed as a map (Figure 6A), which shows the homogeneity of the mean lifetime distributions on glass surface and colloid-coated surface, respectively. These average lifetime distributions (Figure 6B) for the colloid-coated part (patterned triangle) and control glass surface (the remaining area) clearly demonstrate a significant decrease in the lifetime on colloid-coated surface.

(47) Goldys, E. M.; Tomsia, K.; Xie, F.; Shtoyko, T.; Matveeva, E.; Gryczynski, I.; Gryczynski, Z. *J. Am. Chem. Soc.* **2007**, *129*, 12117.

We now discuss the lifetime results within the framework of conventional theories. These predict that the lifetime τ is given by:[14]

$$\tau = (\Gamma + k_{nr})^{-1} \quad (3)$$

where Γ and k_{nr} are the radiative and nonradiative decay rate, respectively. The value of k_{nr} are typically affected by a fluorophore's environment, which may induce quenching or fluorescence resonance energy transfer (FRET),[14] whereas the radiative decay rate Γ is an intrinsic property of a fluorophore. These allow us to calculate the fluorescence quantum yield (Q), which is the ratio of the radiative rate to the total decay rate

$$Q = \Gamma/(\Gamma + k_{nr}) \quad (4)$$

The proximity of fluorophore to metals results in an increase in the total radiative decay rate by addition of a new rate Γ_m to the emission rate Γ applicable to the free space conditions.[14] The modified fluorescent lifetime (τ_m) and quantum yield (Q_m) are then given by

$$\tau_m = (\Gamma + \Gamma_m + k_{nr})^{-1} \quad (5)$$

$$Q_m = (\Gamma + \Gamma_m)/(\Gamma + \Gamma_m + k_{nr}) \quad (6)$$

The effect of proximity of the metal on k_{nr} is negligible.[14] By using the measured fluorescence lifetime ratios of Deep Purple on gold colloid and clean glass surface (eqs 3 and 5) and using the quantum yield of Deep Purple bound to BSA in free-space conditions of 0.2[5] (eq 4), we were able to obtain the value of Γ_m/Γ and hence the emission enhancement (E_{em}), defined as $E_{em} = Q_m/Q$, for each sample. These are listed in Table 1. The excitation enhancement (E_{ex}) for each sample is calculated by dividing the (total) fluorescence enhancement factor (E_t) by the emission enhancement (Q_m/Q), given by

$$E_{ex} = E_t/E_{em} \quad (7)$$

The values are listed in Table 2.

Table 1 shows that the fluorescence lifetimes for the fluorophores deposited on the metallic surfaces are reduced compared to the measured fluorescence lifetime of Deep Purple deposited on a pure glass surface of 2.6 ns. The

radiative decay rates are significantly increased and likewise the quantum yields of the fluorophore. The shortest observed lifetime for the fluorophore monolayer on the 162 nm Au colloid with 24 h incubation is 300 ps, which is well within the range of experimental capabilities and accuracy because the fluorescence lifetime system response is on the order of 30 ps.

Now we discuss the results for 2 h incubation time. For such samples, the τ/τ_m values (Table 1) increase from 2.4 to 4.1 with increasing colloid size. Consequently, the emission enhancement, $E_{em} = Q_m/Q$, increases from 3.35 to 4.00. However, the excitation enhancement factor E_{ex} remains practically constant; and varies only slightly from 1.70 to 1.88 with increasing colloid size (Table 2). This is because for well isolated Au nanoparticles, there is negligible coupling between nanoparticles and thus no amplification of the exciting electromagnetic field. Consequently, the nanoparticle size has no further effect on the excitation enhancement. In contrast, the Au colloid size plays a significant role in the emission enhancement. This is apparent in the radiative decay rate induced by metal, Γ_m, which increases significantly with increasing Au colloid size. Likewise the quantum yield on metallic surface increases from 0.67 to 0.8, as shown in Table 1.

We further analyze the results for 24 h incubation time. The total fluorescence enhancement increases significantly compared with the data for 2 h incubation (Table 2) when the interparticle distance is reduced. This clearly suggests that the interparticle distance is a significant factor in the total fluorescence enhancement. The lifetime results make it possible to investigate its impact on excitation and emission enhancements individually. From the data listed in Table 1 for 24 h incubation, the τ/τ_m values are 7.2, 8.6, and 8.9 for 80, 118, and 162 nm Au colloid, respectively. Surprisingly, contrary to the results for 2 h deposition, the corresponding emission enhancement, $E_{em} = Q_m/Q$, increases only from 4.40 to 4.55 with increasing Au colloid size. The quantum yields Q_m of fluorophore on these metallic surfaces increase from 0.89 to 0.91, with increasing Au colloid size (Table 1), suggesting that the colloid size effect is not important any more. We note that these values of Q_m are close to unity, the maximum quantum yield which could be achieved by a fluorophore. Because the quantum yield is so close to its maximum saturation value, the influence of size is not as pronounced as in the case of 2 h deposition, where the quantum yields are lower and further from saturation. However, appreciable size effects could still be possible for smaller colloids and lower quantum yield fluorophores. In our case, the combined effect from both size of Au colloid and the interparticle distance causes the emission enhancement to reach its plateau. This is also clearly seen in the values of relative quantum yield Q_m/Q of the fluorophore on the metallic surfaces (Table 1), which are approaching the value of 5, which is the maximum theoretical value of the emission enhancement for a Deep Purple fluorophore with quantum yield of 0.2. The excitation enhancements of the samples with decreased interparticle distances for 24 h deposition have been examined as well. The excitation enhancement factors are 2.1, 2.6, and 3.5 for 80, 118, and 162 nm Au colloids, respectively. They vary significantly both as a function of colloid size and interparticle distances. As discussed earlier, the size effect on the excitation enhancement is minor when the nanoparticles are isolated due to negligible electromagnetic field coupling and the resulting absence of strong localized electromagnetic fields. Thus, in this regime, the particle size and local field enhancement are not related. However, when interparticle distances are reduced, the enhancement of local electromagnetic fields intensity becomes strong[48] which magnifies the excitation enhancement induced by these nanoparticles. In this regime, the local electromagnetic field strength decreases with particle size. In summary, both size and interparticle distance play a significant role in the total fluorescence enhancement induced by metal, and fluorescence can be dramatically enhanced when the particles of appropriate size are brought close enough to enable the effective coupling and localization of the electromagnetic field. We also noticed that there was only little variation of the enhancement factors under each condition between corresponding different samples, respectively. It suggests that the substrates with various sizes of Au colloidal nanoparticles with different interparticle distances are highly reproducible, with which pave the way for its potential applications in biosensors.

Conclusion

The fluorescence enhancement induced by homogeneous Au self-assembled nanoparticle monolayers was observed and investigated. Au colloids 40, 59, and 81 nm in radius were homogeneously deposited on glass substrates with two different densities and varying interparticle coupling. The fluorescence spectra of FITC-HSA and DP-BSA on metallic surface show a varying level of fluorescence enhancement depending on Au colloid size and coverage of the metal nanoparticles. The origin of the observed enhancement is attributed to an increased excitation rate from the local field enhanced by the interaction of incident light with the nanoparticles and higher quantum yield from an increase of the intrinsic decay rate of the fluorophore. Our results show that the fluorescence enhancement in the samples with dense packed Au colloid monolayers is generally much higher than that from the well-isolated nanoparticles. The fluorescence lifetime data from the DP-BSA monolayer indicate that for the well-isolated nanoparticles the overall fluorescence enhancement is dominated by the emission enhancement. In this regime both emission and total fluorescence enhancement depend strongly on nanoparticle size. The situation is different when the nanoparticles are closely packed, which enables effective localization of electromagnetic field in interparticle regions. For such close nanoparticles even if the emission enhancement reaches its plateau, the excitation enhancement can be further increased as small interparticle distance lead to the effective coupling of the localized field. In this case, both particle size and interparticle distances become significant factors in the fluorescence enhancement, producing appreciable enhancement values on the order of 15 demonstrated here.

(48) Li, K.; Stockman, M. I.; Bergman, D. J. *Phys. Rev. B* **2005**, *72*, 153401.

We have thus shown that Au colloids with appropriate size and optimized interparticle distance can produce promising substrates for fluorescence enhancement with outstanding macroscopic homogeneity. The work presented here has implications for ultrasensitive bioassays with improved detectability of biomolecules bound to surfaces with Au colloid monolayers.

Acknowledgment. F.X. acknowledges financial support from Macquarie University RAACE (Research Areas and Centers of Excellence Award) Scholarship and the Macquarie University Biotechnology Research Institute (MUBRI).

CM703121M

(49) http://www.sigmaaldrich.com.